Ultra-Reliable Device-Centric Uplink Communications in Airborne Networks: A Spatiotemporal Analysis

Yasser Nabil, Hesham ElSawy, Suhail Al-Dharrab, Hussein Attia, and Hassan Mostafa

Abstract—This paper proposes an ultra-reliable device-centric uplink (URDC-UL) communication scheme for airborne networks. In particular, base stations (BSs) are mounted on unmanned aerial vehicles (UAVs) that travel to schedule UL transmissions and collect data from devices. To attain an ultra-reliable unified device-centric performance, the UL connection is established when the UAV-BS is hovering at the nearest possible distance from the scheduled device. The performance of the proposed URDC-UL scheme is benchmarked against a stationary UAV-centric uplink (SUC-UL) scheme where the devices are scheduled to communicate to UAV-BSs that are continuously hovering at static locations. Utilizing stochastic geometry and queueing theory, novel spatiotemporal mathematical models are developed, which account for the UAV-BS spatial densities, mobility, altitude, antenna directivity, ground-to-air channel, and temporal traffic, among other factors. The results demonstrate the sensitivity of the URDC-UL scheme to the ratio between hovering and traveling time. In particular, the hovering to traveling time ratio should be carefully adjusted to maximize the harvested performance gains for the URDC-UL scheme in terms of link reliability, transmission rate, energy efficiency, and delay. Exploiting the URDC-UL scheme allows IoT devices to minimize transmission power while maintaining unified reliable transmission. This preserves the device's battery and addresses a critical IoT design challenge.

Index Terms—Airborne networks, device-centric networks, ultra-reliable uplink communication, Internet of Things (IoT), unmanned aerial vehicles (UAVs), spatiotemporal model, stochastic geometry, queueing theory.

I. INTRODUCTION

AIRBORNE networks are envisioned as a fundamental pillar for 5G and beyond systems [1]–[4]. Airborne networks may comprise multi-altitude aircraft platforms that carry base stations (BSs) to provide comprehensive and ubiquitous wireless services. In particular, airborne networks include low-orbit satellite constellations, high-altitude platforms (HAPs), and low-altitude platforms (LAPs) [5]–[8]. Such emerging

Y. Nabil is with the Department of Electronics and Communication Engineering, Cairo University, Giza 12613, Egypt, e-mail: Yasser.202010367@eng-st.cu.edu.eg.

H. ElSawy is with the School of Computing, Queen's University, Kingston, ON, Canada, e-mail: hesham.elsawy@queensu.ca.

S. Al-Dharrab and H. Attia are with the Electrical Engineering Department, and the Center for Communication Systems and Sensing at King Fahd University of Petroleum & Minerals (KFUPM), Dhahran, 31261, Saudi Arabia, e-mails: {suhaild, hattia}@kfupm.edu.sa.

H. Mostafa is with the Department of Electronics and Communication Engineering, Cairo University, Giza 12613, Egypt, and also with the University of Science and Technology, Nanotechnology and Nanoelectronics Program, Zewail City of Science and Technology, Giza 12578, Egypt, e-mail: hmostafa@staff.cu.edu.eg

airborne networking paradigm offers several benefits which include extending wireless network connectivity to rural places, providing rapid network deployment in case of disasters, aggregating data from massive Internet of Things (IoT) devices, and improving the overall network resilience [9], [10]. In addition, aerial BSs enhance wireless communication performance and provide a flexible network architecture that can adapt to real-time traffic variations [11], [12].

Concurrently, device-centric communication architectures are viewed as a crucial approach for future wireless networks, particularly IoT Networks [13], [14]. In device-centric networks, the device's performance is of critical importance, with fairness among devices as the most significant characteristic [13], [14]. Using the mobility capabilities of unmanned aerial vehicles (UAVs), they can travel between devices in order to reduce performance disparities between them. In the case of UAVs, the device-centric design will not only provide a short connection distance, but also a very high line-of-sight (LOS) probability for the link between devices and UAVs. This can finally lead us to the ultra-reliable transmission [15]. Inspired by the spatiotemporal models in [16]–[18], this paper utilizes stochastic geometry and queuing theory to characterize device-centric ultra-reliable uplink transmission in large-scale airborne networks. The developed model account for the impact of aggregate interference on transmission reliability, energy efficiency, and delay.

A. Related Work

UAVs are among the most common LAPs, which are considered to be agile, low-cost, and easy to deploy [19]–[23]. Such foreseen merits have motivated the academic and industrial societies to propose the UAV-BSs utilization and assess their performance for various application in 5G and beyond systems. For instance, the authors in [24] exploit the UAV agility to optimize their locations in response to the real-time device's activity to minimize the uplink transmission power. The authors in [25] utilize UAVs to provide downlink services to a rural region with no terrestrial BSs coverage. The uplink data aggregation scenario from IoT devices in rural areas is considered in [26]. In both [25], [26] the trajectory and hovering locations for the UAV are optimized to minimize the trip time to circulate the service area. Instead of using a single UAV, the authors in [27] proposed a fleet of UAVs to gather data from IoT devices that begin transmission whenever they are inside a UAV's coverage area. In [28], UAVs are used as

downlink sky-haul relays to connect IoT devices to the internet through satellites.

Wireless power transfer from UAVs to IoT devices to enhance battery life or enable local computation is proposed in [29], [30]. Moreover, joint optimization of performance metrics for a hovering UAV that offers edge services for mobile users is presented in [31]. The Age of Information (AoI) minimization for UAV-aided edge computing is presented in [32]–[34]. The coexistence of UAVs with conventional terrestrial BSs is studied in [35], [36]. In [35], terrestrial backhauled UAV-BSs are utilized to improve the coverage of cellular devices. In [36], the UAVs are used to aggregate data from IoT devices and the terrestrial BSs are used to provide conventional cellular service. The authors in [37] utilize UAVs to compensate for destroyed terrestrial BSs to maintain coverage during disasters. The negative impact of the limited battery power on the UAV-BS service is quantified in [38]. To overcome such power constraints, the authors in [39] proposed a laser-powered UAV operation. Tethered UAV-BSs are investigated in [40] as an alternative solution for the limited UAV battery lifetime problem. Such a tether provides a perpetual energy source and reliable high-bandwidth backhaul for UAVs at the cost of limiting their mobility. In [41] serving UAVs are charged on the fly to increase the travel time.

In addition to the aforementioned use cases, UAV-BSs are promoted to offer ultra-reliable communication services [15]. Adapting UAV locations and altitudes, ultra-reliable line-of-sight (LOS) communication links can be established as proposed in works listed in Table I. However, to attain the required 99.999% transmission success probability [42], [43], interference from other UAVs and devices has to be considered. In all the works that studied ultra-reliable transmission through UAVs, stochastic geometry analysis that can characterize interference in large-scale networks is missing. In addition, in the same context, the spatiotemporal models are overlooked, whereas, in this paper, we try to close this gap.

B. Contributions

This paper studies aerial data aggregation in large-scale IoT networks, where dynamic device-centric and stationary UAV-centric network scenarios are considered. The former is denoted as an ultra-reliable device-centric uplink (URDC-UL) scheme, where each UAV-BS travels to schedule uplink transmissions and collect data from IoT devices with better LOS conditions, but an amount of time is wasted on physical movement. In contrast, the latter is denoted as a stationary UAV-centric uplink (SUC-UL) scheme, where each UAV-BS stays at a fixed location to schedule the uplink transmissions. Here all the time is dedicated to transmission but subjected to a higher transmission failure. It is shown that the URDC-UL scheme outperforms the SUC-UL in terms of reliability, rate, energy efficiency, delay, and fairness. More importantly, by virtue of the URDC-UL scheme, the devices can operate at very low transmit power and rarely experience decoding errors,[1] which improves energy efficiency and extends the battery

lifetime of the devices. In summary, the main contributions of this paper compared to the previously mentioned works are summarized as follows.

- It presents a novel device-centric spatiotemporal mathematical model for data aggregation in large-scale IoT networks via UAVs, with trajectory planning taken into account.
- It employs stochastic geometry to examine the ultra-reliable transmission perspective through UAVs in large-scale networks while considering interference from other UAVs and devices.
- It accounts for the UAVs' mobility for ultra-reliable data aggregation from IoT devices. This can extend the device's battery lifetime, in addition to achieving fairness between devices through the device-centric approach.

The remainder of the paper is divided as follows: Section II introduces the URDC-UL and SUC-UL system models. Section III presents the transmission success probability analysis. Section IV presents the temporal analysis, and some performance metrics such as outage capacity and energy efficiency. Section V presents the numerical results and simulations. Finally, Section VI concludes and summarizes the work.

II. System Model

This section describes the system model for both the URDC-UL scheme and the SUC-UL benchmark. We first introduce the considered network parameters including the aerial channel and antennas models. Following that, the temporal and transmission models for the URDC-UL and the SUC-UL schemes are presented.

A. Network Model

An infinite network is considered where IoT devices are distributed according to a Poisson point process (PPP) defined as $\Phi_d = \{d_i \in \mathbb{R}^2, \forall i \in \mathbb{N}^+\}$ with intensity λ_d device/km^2. This PPP placement of devices will effectively cover the entire area and provide some redundant sensing in case a node fails [26]. A homogeneous coverage is adopted for aerial uplink services, where the network is partitioned via a hexagonal tessellation with hexagons of radii R. Each UAV-BS is assigned to serve the devices within each hexagonal cell. While the area served by each UAV is fixed by design and based on the definition of PPP [55], the number of devices per each hexagonal cell is independent and follows a Poisson distribution with mean N. Such that N equals to the cell area multiplied by λ_d, i.e. $N = \frac{3\sqrt{3}\lambda_d R^2}{2}$. Devices have negligible heights and UAV-BSs are flying at a constant altitude of h.

Aerial communication is characterized by complex propagation conditions, where obstacles in environments may lead to deep shadow areas and the absence of LOS. In particular, the probability of a LOS link depends on the ratio of built-up land area to the total area, the average number of buildings per km^2, and buildings' height distribution. Such LOS probability is well-approximated by a modified Sigmoid function with proper environment parameters [56], given by

---

[1]Decoding errors lead to packet retransmissions resulting in higher power consumption.

$$p_{\text{LOS}}(r) = \frac{1}{1 + a \, \exp\left(-b\left(\frac{180}{\pi}\arctan\left(|\frac{h}{r}|\right) - a\right)\right)}, \quad (1)$$

TABLE I: Ultra-reliable UAV efforts

Reference	Scope	Network scale	Interference analysis
[44]	compute the average probability of packet error and effective throughput for short control packets to UAV	single link	No
[45]	optimize the height and bandwidth allocation to reduce the total bandwidth requirement	multi-cell	No
[46]	optimize the locations of UAVs and device associations to reduce the total transmit power of the IoT devices	single-cell	No
[47]	optimize locations of UAVs carrying reconfigurable intelligent surface (RIS) to reflect the signal from BS to far users	macro cell with relay clusters	only intra-cluster
[48]	UAV-BS serve ground users in the downlink, considering altitude-dependent path loss exponent and fading function	single-cell	No
[49]	optimize distance and the blocklength of multi-hop downlink between two IoT devices using UAVs relays	multi-hop relay links	No
[50]	beamwidth optimization for downlink UAV-assisted non-orthogonal multiple access (NOMA)	single-cell with multiple groups	only intra-group
[51]	optimize location, height, beamwidth, and resource allocation for a relay UAV between a controller and mobile robots	single-cell with relay link	No
[52]	optimize the UAVs' height, uplink and downlink duration, and antenna configuration to maximize the horizontal distance between UAVs and a ground station	multi-UAV network	No
[53]	UAVs offer edge computing offloading for IoT devices while optimizing UAVs locations, resource allocation, and offloading decisions	multi-UAV network	No
[54]	jointly optimize resource allocation for both payload and ultra-reliable control links in a multi-UAV relay network	single-cell multi-UAV relay network	only for payload links

where a and b denote environment parameters, and r is the ground Euclidean distance between the UAV and the device.

The uplink propagation channel between devices and UAVs has a distance-dependent power-law path loss function with different exponents, α_L and α_N for LOS and none LOS (NLOS) channels, respectively. We assume a quasi-static Nakagami-m multipath fading model where the channel gains remain constant during one transmission duration but randomly change across different transmissions. All power fading gains are modeled as independent and identically distributed (i.i.d.) Gamma random variables (RVs) with shape parameters m_L and m_N for LOS and NLOS, respectively. Note that $\alpha_L < \alpha_N$ and $m_L > m_N$, reflect the better LOS channel conditions when compared to their NLOS counterpart.

Universal frequency reuse of W Hz is adopted by all UAV-BSs and devices transmitted with a constant power of P. To improve the intended signal and mitigate interference, both the UAVs and devices are equipped with directional antennas. For simplicity, the antenna patterns of the UAVs and devices are approximated with the discretized sectored gain model adopted in [57], [58]. In particular, the main lobe and side lobe gains of the UAV antennas are denoted by G_{uM} and G_{um}, respectively. Similarly, the main lobe and side lobe gains of the device's antennas are denoted by G_{dM} and G_{dm}, respectively. Note that the case of simple devices with Omni-directional antennas is captured by a special case of $G_{dM} = G_{dm} = 1$. Perfect beam alignment is assumed between a UAV-BS and its intended devices in both the URDC-UL and the SUC-UL schemes. However, the orientation of the interfering devices beams with respect to other UAVs is assumed to be random with uniform distribution

in the range $(0, 2\pi)$. Hence, the beamforming effect between a UAV and interfering devices can be modeled via i.i.d. discrete RVs $G \in \{G_{dM}G_{uM}, \ G_{dM}G_{um}, \ G_{dm}G_{uM}, \ G_{dm}G_{um}\}$, which has a probability mass function $\mathbb{P}\{G = G_{d\{\cdot\}}G_{u\{\cdot\}}\} \in \{c_d c_u, \ c_d(1 - c_u), \ (1 - c_d)c_u, \ (1 - c_d)(1 - c_u)\}$ such that $c_d = \frac{\theta_d}{2\pi}$ and $c_u = \frac{\theta_u}{2\pi}$, where θ_d and θ_u are the main lobe beamwidth for devices and UAVs.

B. Transmission and Temporal Model

We consider a time-slotted system with time slot duration T_s, where each device generates a packet of size L bits with probability α every time slot[2]. In addition, each device has a buffer that stores generated packets to be transmitted to its serving UAV according to the first in first out (FIFO) discipline. The UAVs schedule the devices to transmit their head of the buffer (HoB) packets according to periodic transmission cycles. For the sake of fairness, each transmission cycle includes all the devices within the service area of each UAV, where each device is scheduled only once[3]. Therefore, the duration of the transmission cycle for a randomly selected UAV is equal to $T_c = N_d \times T_s$, where N_d is the number of devices within the service area of the selected UAV. Note

---

[2]The developed model can be extended to other traffic generation models as in [59].

[3]A queue-aware scheduling assumption is technically challenging in the considered uplink scenario because the UAV may be oblivious of the queue states of the devices. Moreover, buffer state updates from devices to UAVs result in additional power consumption and signaling overhead [60], [61]. Instead and to void wasting of resources, if the assigned device has an empty buffer, it is assumed that it will transmit additional secondary data that is not included in queueing analysis. Consequently, there is always transmission and interference at each time slot from all cells.

that N_d has a Poisson distribution, with mean N, across different UAVs. The scheduling and transmission policies for both schemes are given in the sequel.

1) SUC-UL scheme: All UAVs remain stationary at the center of their service area and the devices are scheduled according to round-robin scheduling as depicted in Fig. 1. Each device exploits the entire slot duration T_s for transmitting the HoB packet. To transmit the packet size of L bits within T_s, the required transmission rate is given by[4]

$$\mathcal{R}_{\text{UC}} = \frac{L}{T_s} = \zeta \, W \, \log_2 \left(1 + \theta_{\text{UC}} \right), \tag{2}$$

where ζ is the rate penalty of using practical coding schemes as opposed to the theoretical Shannon capacity. θ_{UC} is the signal-to-interference-plus-noise-ratio (SINR) threshold required to correctly decode the packet at the UAV. Hence, the transmitted packet is correctly received at the serving UAV if the received SINR satisfies

$$\text{SINR}_{\text{UC}} \geq \theta_{\text{UC}} = 2^{\frac{L}{T_s \zeta \, W}} - 1. \tag{3}$$

2) URDC-UL scheme: A trajectory planning is required for the UAV to travel, schedule the devices and collect HoB packets. For simplicity, a greedy scheduling trajectory is employed for the URDC-UL scheme[5]. In particular, the UAV trajectory starts at a randomly selected device and passes in a hop-by-hop fashion by all devices within the service area of the UAV. At each hop, the nearest unscheduled device is selected as the next hop in the trajectory, and thus, each device is scheduled once every transmission cycle as shown in Fig. 2. Due to practical and environmental constraints and/or possible errors in the localization, sometimes it could be hard for the UAV to hover directly above the device. Thus, the horizontal distance between the UAV and the selected device is assumed not to be zero but is modeled as a Gaussian RV with a zero mean and standard deviation (SD) η.

The URDC-UL scheme activates a device for uplink transmission once the UAV arrives at its corresponding hop. Hence, there is the time consumed by the UAV to travel between the devices, where all the devices in the cell remain silent. For the sake of fair comparison, the transmission cycle duration, T_c, is fixed for both the URDC-UL and SUC-UL schemes, where all the devices have to be scheduled. Hence, each device in the URDC-UL is granted $t_{\text{DC}} < T_s$ for packet transmission. In particular, the total UAV travel time and the total transmission time have to satisfy $\sum_{i=0}^{N_d - 1} t_{v,i} + N_d \times t_{\text{DC}} = N_d \times T_s = T_c$, where N_d is the number of devices served by a UAV and $t_{v,i}$ is the time it takes the UAV to travel the ith segment of the trajectory. Note that t_{DC} is fixed for all devices for the sake of fairness, however, $t_{v,i}$ varies according to the trajectory and the relative locations of devices. Due to the shorter duration allocated to transmit a packet of the same size L, the URDC-UL devices have to operate at a higher rate when compared

to their SUC-UL counterpart. The required transmission rate for the URDC-UL scheme is

$$\mathcal{R}_{\text{DC}} = \frac{L}{t_{\text{DC}}} = \zeta \, W \, \log_2 \left(1 + \theta_{\text{DC}} \right). \tag{4}$$

Hence, the URDC-UL has a more strict SINR threshold which is given by

$$\text{SINR}_{\text{DC}} \geq \theta_{\text{DC}} = 2^{\frac{L}{t_{\text{DC}} \zeta \, W}} - 1. \tag{5}$$

In both the URDC-UL and the SUC-UL, packets correctly received at the UAV are omitted from the buffer. Otherwise, the HoB packet is retransmitted until it is successfully delivered.

Remark 1: While the URDC-UL scheme devices are assigned shorter transmission slots and are required to operate at higher rates, they are privileged with better channel conditions including high LOS probability and shorter transmission distance when compared to the SUC-UL scheme. Since the LOS links experience less attenuation and/or multipath fading, the URDC-UL scheme offers higher reliability and enables the devices to operate with lower power, which prolongs their battery lifetime.

III. TRANSMISSION SUCCESS PROBABILITY ANALYSIS

In this section, the transmission success probability for both the URDC-UL and SUC-UL schemes is formulated.

A. URDC-UL

Due to the fact that each UAV serves a single device during each time slot, there could only be one interfering device per hexagonal cell. Note that the travel and transmission time slots of UAVs in different cells are not synchronized due to the different lengths of the trajectory segments in different cells. Hence, the transmission activities of the interfering devices are not synchronized. As such, we adopt the following approximation for the interference devices.

Approximation 1: Without loss of generality, consider the serving UAV-BS that schedules a typical device to be located at the origin. To ensure mathematical tractability, the interfering devices for a typical device in the URDC-UL are approximated with a PPP[6] $\boldsymbol{\Phi} = \{x_i \in \mathbb{R}^2, \forall i \in \mathbb{N}^+\}$ of intensity

$$\lambda_{\text{DC}} = \frac{t_{\text{DC}}}{T_s} \times \frac{2}{3\sqrt{3}R^2}. \tag{6}$$

The intensity in (6) is equivalent to that of the hovering UAV-BSs, where the term $\frac{t_{\text{DC}}}{T_s}$ captures the asynchronous transmission. Furthermore, due to the absence of intra-cell interference and the fact that two active devices may simultaneously exist at the margins of two adjacent cells, but at the same time other neighboring interference devices will be located at distances far greater than the cell radius, R. Therefore, the interfering devices are assumed to exist outside an interference-free region, which is approximated via a circle of radius $\frac{R}{2}$ around the origin. This strikes a compromise between the two extreme cases of no interference protection region at all and the case of an unrealistically large protection region with a radius of

---

[4]Hereafter, the subscripts UC and DC are used to denote, respectively, the UAV centric (i.e., SUC-UL) and the device-centric (i.e., URDC-UL) schemes.

[5]Trajectory optimization is a stand-alone problem that is out of the scope of this paper. The main objective of this work is to assess the impact of device-centric uplink scheduling as opposed to the stationary UAV-centric approach. In this context, the gains offered by the URDC-UL scheme will be enhanced if trajectory optimization or clustered user techniques are deployed
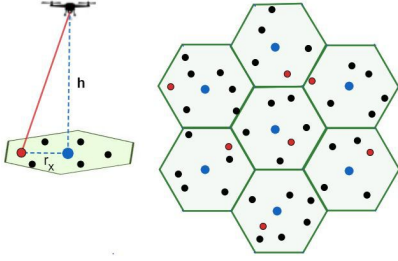
[6]The PPP approximation of interferers can cover other scenarios even if devices' spatial deployment is not PPP as in [18].

Fig. 1: The SUC-UL scheme for $N = 6$ (filled circles in blue: UAV fixed locations, red: active devices, black: inactive devices).
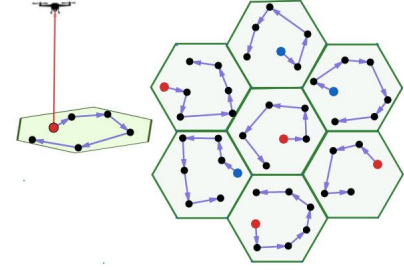

Fig. 2: The URDC-UL scheme for $N = 6$ (filled circle in blue: traveling UAV, red: UAV hovering close to an active device, and arrows show the trajectory).

R. The accuracy of this approximation will be evaluated in section V of numerical results.

The SINR of the typical device is

$$\text{SINR}_{\text{DC}} = \frac{PH_{k,o}G_{dM}G_{uM}(r_x^2 + h^2)^{\frac{-\alpha_k}{2}}}{I_L + I_N + \sigma^2}, \quad (7)$$

where $k \in \{L, N\}$ is an indicator that depends on whether the intended link is LOS or NLOS, r_x is the typical device horizontal distance from the origin which is a RV, $H_{k,o}$ is the intended device channel fading gain, P is the device transmission power, σ^2 is the noise power, and I_L (resp. I_N) is the LOS (resp. NLOS) interference. The LOS and NLOS interference are given by

$$I_L = \sum_{x_i} \mathbb{1}_{\{x_i \in \Phi_L\}} PH_{L,i}G_{\epsilon,i}(r_i^2 + h^2)^{\frac{-\alpha_L}{2}},$$

$$I_N = \sum_{x_i} \mathbb{1}_{\{x_i \in \Phi_N\}} PH_{N,i}G_{\epsilon,i}(r_i^2 + h^2)^{\frac{-\alpha_N}{2}},$$

where $H_{L,i}$ (resp. $H_{N,i}$) is the channel gain of the ith LOS (resp. NLOS) interfering device, and r_i is the horizontal distance between device x_i and the origin. Φ_L is the PPP of LOS interfering devices with intensity $p_{\text{LOS}}(r) \times \lambda_{\text{DC}}$, while Φ_N is the PPP of NLOS interfering devices with intensity $(1 - p_{\text{LOS}}(r)) \times \lambda_{\text{DC}}$, and $p_{\text{LOS}}(r)$ is given by (1). $G_{\epsilon,i}$ is the device x_i interference antennas gain. $G_{\epsilon,i} \in \{G_{dM}G_{uM}, G_{dM}G_{um}, G_{dm}G_{uM}, G_{dm}G_{um}\}$ with probability $\mathbb{P}_\epsilon \in \{c_d c_u, c_d(1 - c_u), (1 - c_d)c_u, (1 - c_d)(1 - c_u)\}$, and $\epsilon \in \{1, 2, 3, 4\}$. The indicator function $\mathbb{1}_{\{\cdot\}}$ takes the value one if the statement $\{\cdot\}$ is true and zero otherwise.

To find the transmission success probability of the URDC-UL scheme, we start by formulating the Laplace transform (LT) of the aggregate interference seen at the typical UAV.

Lemma 1: For the URDC-UL model, the LT of the aggregate LOS and NLOS interference seen by the typical UAV located at the origin is given by (8) and (9) respectively.

$$\mathcal{L}_{I_L}(s) = \exp\left\{-2\pi\lambda_{\text{DC}}\sum_{\epsilon=1}^{4}\mathbb{P}_\epsilon\int_{\frac{R}{2}}^{\infty} p_{\text{LOS}}(r)\right.$$
$$\left.\left(1 - \left(1 + \frac{sPG_\epsilon(r^2 + h^2)^{\frac{-\alpha_L}{2}}}{m_L}\right)^{-m_L}\right)rdr\right\}. \quad (8)$$

$$\mathcal{L}_{I_N}(s) = \exp\left\{-2\pi\lambda_{\text{DC}}\sum_{\epsilon=1}^{4}\mathbb{P}_\epsilon\int_{\frac{R}{2}}^{\infty} (1 - p_{\text{LOS}}(r))\right.$$
$$\left.\left(1 - \left(1 + \frac{sPG_\epsilon(r^2 + h^2)^{\frac{-\alpha_N}{2}}}{m_N}\right)^{-m_N}\right)rdr\right\}. \quad (9)$$

Proof: See Appendix A. ∎

Using the results of Lemma 1, the packet success probability can be formulated as in the following theorem.

Theorem 1: For the URDC-UL model, the packet success probability is given by

$$S_p = \int_{-\infty}^{\infty} [(S_p|k = L)\, p_{\text{LOS}}(r_x) + (S_p|k = N)$$
$$(1 - p_{\text{LOS}}(r_x))]\frac{1}{\sqrt{2\pi\eta^2}}\exp\left(\frac{-r_x^2}{2\eta^2}\right)dr_x, \quad (10)$$

where $p_{\text{LOS}}(r_x)$ is the probability that the intended link is LOS given by (1), and

$$(S_p|k) = \sum_{n=1}^{m_k}(-1)^{n+1}\binom{m_k}{n}\exp\left(-\frac{g_k\, n\, \theta_{\text{DC}}\,(r_x^2 + h^2)^{\frac{\alpha_k}{2}}\sigma^2}{PG_{dM}G_{uM}}\right)$$
$$\mathcal{L}_{I_L}\left(\frac{g_k\, n\, \theta_{\text{DC}}\,(r_x^2 + h^2)^{\frac{\alpha_k}{2}}}{PG_{dM}G_{uM}}\right)\mathcal{L}_{I_N}\left(\frac{g_k\, n\, \theta_{\text{DC}}\,(r_x^2 + h^2)^{\frac{\alpha_k}{2}}}{PG_{dM}G_{uM}}\right). \quad (11)$$

$\mathcal{L}_{I_L}, \mathcal{L}_{I_N}$ are given by (8), (9), $g_L = m_L(m_L!)^{-\frac{1}{m_L}}$ and $g_N = m_N(m_N!)^{-\frac{1}{m_N}}$.

Proof: See Appendix B. ∎

The success probability calculated above is the average. In order to have a detailed characterization of the performance experienced by the devices, the meta-distribution is considered. It is defined as $\overline{F}_{S_p}(X) = \mathbb{P}(S_p(\theta_{DC}) > X)$, where $X \in [0, 1]$. The meta distribution identifies the fraction of devices having success probability at SINR threshold θ_{DC} with reliability X. According to [62] and utilizing the Gil-Pelaez theorem [63], the meta distribution is given by

$$\overline{F}_{S_p}(X) = \frac{1}{2} + \frac{1}{\pi}\int_0^{\infty}\frac{\Im\left(e^{-jt\log X}M_{jt}(\theta_{DC})\right)}{t}dt, \quad (12)$$

where $\Im(f)$ is the imaginary part of f, $j \triangleq \sqrt{-1}$ and $M_{jt}(\theta_{DC})$ are the imaginary moments of the packet success probability at SINR threshold θ_{DC}.

Following similar steps as in [64] and utilizing our system parameters, the bth moment of the packet success probability

at SINR threshold θ_{DC} is given by

$$M_b(\theta_{DC}) = \sum_{z=0}^{b} (-1)^z \binom{b}{z} \int_{-\infty}^{\infty} \left[z_L\, p_{\mathrm{LOS}}^b(r_x) + \right.$$
$$\left. z_N\, (1 - p_{\mathrm{LOS}}(r_x))^b \right] \frac{1}{\sqrt{2\pi\eta^2}} \exp\left(\frac{-r_x^2}{2\eta^2}\right) dr_x, \tag{13}$$

where

$$z_k = \sum_{n=0}^{m_k z} (-1)^n \binom{m_k z}{n} \exp\left(- \frac{g_k\, n\, \theta_{DC}\, (r_x^2 + h^2)^{\frac{\alpha_k}{2}}\, \sigma^2}{PG_{dM}G_{uM}}\right)$$
$$\mathcal{L}_{I_L}\left(\frac{g_k\, n\, \theta_{DC}\, (r_x^2 + h^2)^{\frac{\alpha_k}{2}}}{PG_{dM}G_{uM}}\right) \mathcal{L}_{I_N}\left(\frac{g_k\, n\, \theta_{DC}\, (r_x^2 + h^2)^{\frac{\alpha_k}{2}}}{PG_{dM}G_{uM}}\right). \tag{14}$$

Note that $M_1(\theta_{DC})$ gives a similar result to the average packet success probability as Theorem 1. Substituting $b = jt$ in (13) and utilizing Newton's generalized binomial theorem, the $M_{jt}(\theta_{DC})$ is given by

$$M_{jt}(\theta_{DC}) = \sum_{z=0}^{\infty} (-1)^z \frac{(jt)_z}{z!} \int_{-\infty}^{\infty} \left[z_L\, p_{\mathrm{LOS}}^{jt}(r_x) \right.$$
$$\left. + z_N\, (1 - p_{\mathrm{LOS}}(r_x))^{jt} \right] \frac{1}{\sqrt{2\pi\eta^2}} \exp\left(\frac{-r_x^2}{2\eta^2}\right) dr_x, \tag{15}$$

where $(.)_z$ is the Pochhammer symbol of falling factorial.

B. SUC-UL

The UAV-BSs in the SUC-UL scheme utilizes the entire time for uplink transmissions. Hence, there is always an active device that is scheduled in each of the hexagonal cells. As such, for simplicity, we utilize Approximation 1 for the interfering devices' locations but with intensity

$$\lambda_{\mathrm{UC}} = \frac{2}{3\sqrt{3}R^2}, \tag{16}$$

and with interference protection region of R. Considering that the typical UAV is hovering at the origin, the SINR of the SUC-UL model is given as in (7), but here r_x is deterministic, not a RV. The LOS and NLOS interference I_L and I_N are similar to the URDC-UL model where Φ_L is the PPP of LOS interfering devices with intensity $p_{\mathrm{LOS}}(r) \times \lambda_{\mathrm{UC}}$, and Φ_N is the PPP of NLOS interfering devices with intensity $(1 - p_{\mathrm{LOS}}(r)) \times \lambda_{\mathrm{UC}}$.

To find the transmission success probability of the SUC-UL scheme, we start by formulating the LT of the aggregate interference seen by the test UAV.

Lemma 2: For the SUC-UL model, the LT of the aggregate LOS and NLOS interference seen by the test UAV located at the origin is given by (17) and (18) respectively.

$$\mathcal{L}_{I_L}(s) = \exp\left\{-2\pi\lambda_{\mathrm{UC}} \sum_{\epsilon=1}^{4} \mathbb{P}_\epsilon \int_{R}^{\infty} p_{\mathrm{LOS}}(r) \right.$$
$$\left. \left(1 - \left(1 + \frac{sPG_\epsilon(r^2 + h^2)^{\frac{-\alpha_L}{2}}}{m_L}\right)^{-m_L}\right) r\, dr\right\}. \tag{17}$$

$$\mathcal{L}_{I_N}(s) = \exp\left\{-2\pi\lambda_{\mathrm{UC}} \sum_{\epsilon=1}^{4} \mathbb{P}_\epsilon \int_{R}^{\infty} (1 - p_{\mathrm{LOS}}(r)) \right.$$
$$\left. \left(1 - \left(1 + \frac{sPG_\epsilon(r^2 + h^2)^{\frac{-\alpha_N}{2}}}{m_N}\right)^{-m_N}\right) r\, dr\right\}. \tag{18}$$

Proof: Same proof as Lemma 1, except λ_{UC} instead of λ_{DC} and integrate from R not $\frac{R}{2}$. ∎

Utilizing the results of Lemma 2, the packet success probability can be formulated as in the following theorem.

Theorem 2: For the SUC-UL model, the packet success probability is given by

$$S_p = (S_p|k = L)\, p_{\mathrm{LOS}}(r_x) + (S_p|k = N)\, (1 - p_{\mathrm{LOS}}(r_x)), \tag{19}$$

where $(S_p|k = L)$ and $(S_p|k = N)$ are given by (11) but θ_{DC} is replaced by θ_{UC}, and $\mathcal{L}_{I_L}$, $\mathcal{L}_{I_N}$ are given by (17) and (18).

Proof: As in the proof of Theorem 1, except r_x, has a fixed value, not a RV. ∎

Similarly, the meta distribution can be calculated for the SUC-UL model as we have done for the URDC-UL scheme.

IV. TEMPORAL ANALYSIS

In this section, the temporal analysis is carried out. This includes the average UAV travel time for the URDC-UL scheme, the transmission rate, delay, and energy efficiency.

A. Average UAV Travel Time

In the URDC-UL scheme, the average traveling time by UAVs during a single time slot is defined as $t_V = \mathbb{E}\left[\frac{1}{N_d} \sum_{i=0}^{N_d - 1} t_{v,i}\right]$. To evaluate the travel time for each segment $t_{v,i}$, the segment length has to be calculated first. However, the exact characterization for the distribution of the segment length is quite complex. Hence, we resort to a simple yet accurate approximation, which is formally stated in the following proposition.

Proposition 1: The average segment length in the trajectory of a typical UAV can be approximated by

$$d_{\mathrm{avg}} \approx \mathbb{E}_{N_d}\left[\frac{1}{N_d} \sum_{i=0}^{N_d - 1} \int_{0}^{\infty} \frac{4\pi(N_d - i)r^2\, e^{\left(-\frac{2\pi(N_d - i)r^2}{3\sqrt{3}R^2}\right)}}{3\sqrt{3}R^2}\, dr\right]$$

$$= \mathbb{E}_{N_d}\left[\frac{1}{N_d} \sum_{i=0}^{N_d - 1} \sqrt{\frac{3\sqrt{3}R^2}{8(N_d - i)}}\right] \tag{20}$$

$$> \frac{1}{N} \sum_{i=0}^{N-1} \sqrt{\frac{3\sqrt{3}R^2}{8(N - i)}}. \tag{21}$$

Proof: The UAV trajectory that passes by the N_d devices is divided into N_d consecutive segments indexed as $i \in \{0, 1, \cdots, N_d - 1\}$. Since the device's locations are random, the length of the ith segment across different UAV trajectories is also random. To take the device's intensity into consideration and to ensure that no device is left behind in each scheduling cycle, the length of the ith segment for a randomly selected UAV trajectory is approximated by the contact distance in a PPP of intensity $\frac{2(N_d - i)}{3\sqrt{3}R^2}$. Averaging across all segments, the average trajectory length is given by

(20). Noting that the function $\left[\frac{1}{N_d}\sum_{i=0}^{N_d-1}\sqrt{\frac{3\sqrt{3}R^2}{8(N_d-i)}}\right]$ in N_d is convex, then Jensen's inequality for convex functions can be applied. Moreover, since N_d has a Poisson distribution with mean N, the expression in (21) can be deduced, which is much simpler than (20). ∎

The accuracy of Proposition 1 is validated in Fig. 3 via Monte Carlo simulations. In each simulation run, N_d devices following the Poisson distribution of mean $N = 100$ are uniformly and randomly scattered over a hexagonal cell of radius R. Starting from an arbitrary location in the cell, the UAV moves towards the closest device among the N_d devices, and the distance for the $i = 0$ segment is recorded. The covered device is eliminated and the UAV moves towards the closest device among the remaining $N_d - 1$ devices to record the length of the $i = 1$ segment. This process is repeated until all N_d devices are covered and the N_d segments' lengths are recorded. The average segment length across the trajectory in each run is then computed. Towards this end, Fig. 3 validates (20) and (21) against the average segment length for trajectories over 5×10^4 simulation runs, which illustrates the accuracy of Proposition 1.
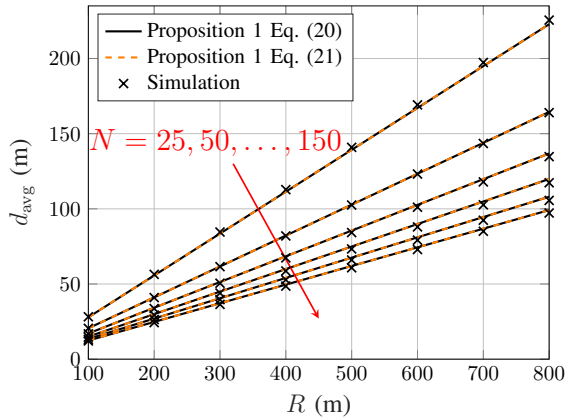

Fig. 3: Average traveling distance at different cell radii.

Applying the equations of motion, then the average traveling time is:

$$t_V = \begin{cases} \sqrt{\frac{d_{\text{avg}}}{a_u+a_d}} & \text{if } d_{\text{avg}} \leq s_u + s_d \\ t_u + t_d + \frac{d_{\text{avg}}-s_u-s_d}{v} & \text{if } d_{\text{avg}} > s_u + s_d \end{cases}, \quad (22)$$

where a_u (resp. a_d) is the UAV acceleration (resp. deceleration), $t_u = \frac{v}{a_u}$ (resp. $t_d = \frac{v}{a_d}$) are the times needed for the UAV to change its speed from 0 to v (resp. v to 0), and $s_u = \frac{1}{2}a_u t_u^2$ (resp. $s_d = \frac{1}{2}a_d t_d^2$) are the distances needed by the UAV to change its speed from 0 to v (resp. v to 0). From t_V, the transmission time for the URDC-UL scheme can be estimated as $t_{\text{DC}} = T_s - t_V$.

B. Transmission Rate & Delay

Here the transmission rate and delay analysis are presented for both models.

1) URDC-UL: The maximum achievable transmission rate is defined by the ergodic capacity $C = \zeta W \mathbb{E}[\log_2(1 + \text{SINR})]$ bits/s. Operating at this rate requires instantaneous

knowledge of the SINR [65]. However, this is not applicable to large-scale IoT networks. Alternatively, a fixed transmission rate, lower than ergodic capacity, that experiences some outages are utilized. In the URDC-UL model, the outage capacity is given by

$$C_{\text{DC}} = \mathbb{P}\left(\text{SINR}_{\text{DC}} > \theta_{\text{DC}}\right) \times \frac{t_{\text{DC}}}{T_s} \times \zeta W \log_2\left(1 + \theta_{\text{DC}}\right), \quad (23)$$

where the multiplicative term $\frac{t_{\text{DC}}}{T_s}$ emphasizes the shorter transmission during t_{DC} when compared to the entire time slot T_s. The matrix analytic method (MAM) [66] is utilized to construct a Geo/PH/1 (see [66, Sec. 5.8]) queueing system at each device, where Geo stands for geometric inter-arrival process and PH stands for the Phase type departure process that accounts for the network dynamics [66]. In particular, geometric inter-arrival times with parameter α are considered at each device. Moreover, since each device attempts to transmit a packet once in each transmission cycle, a PH-type distribution is used to track the round-robin scheduling consisting of N_d time slots, then to capture the probabilistic transmission which is SINR-dependant. Such traffic departure PH type distribution is defined by the initialization vector $\boldsymbol{\beta} = \begin{bmatrix} 1 & 0 & 0 & \cdots & 0 \end{bmatrix}$ of size $1 \times N_d$, transient transition matrix $\mathbf{S}$ of size $N_d \times N_d$ and an absorption vector $\mathbf{s}$ of size $N_d \times 1$, given by

$$\mathbf{S} = \begin{bmatrix} 0 & 1 & 0 & \cdots & 0 \\ 0 & 0 & 1 & \cdots & 0 \\ \vdots & \vdots & \ddots & \ddots & \vdots \\ 0 & 0 & \cdots & 0 & 1 \\ 1-S_p & 0 & 0 & 0 & 0 \end{bmatrix} \quad \text{and} \quad \mathbf{s} = \begin{bmatrix} 0 \\ 0 \\ \vdots \\ 0 \\ S_p \end{bmatrix}, \quad (24)$$

where S_p is the packet transmission success probability calculated in Theorem 1 for the SINR threshold given by (5).

The Geo/PH/1 queueing model has state-space (q, d), where $q \in \mathbb{N}$ is the number of packets in the buffer and $d \in \{0, 1, \cdots, N_d\}$ is the number of time slots that elapsed since the last transmission attempt.

Owing to the fact that only one packet can arrive and/or depart during any time slot, the developed Geo/PH/1 model is a quasi-birth-death (QBD) process with a transition matrix

$$\mathbf{P} = \begin{bmatrix} \mathbf{B} & \mathbf{C} & \mathbf{0} & \mathbf{0} & \mathbf{0} & \cdots \\ \mathbf{E} & \mathbf{A_1} & \mathbf{A_0} & \mathbf{0} & \mathbf{0} & \ddots \\ \mathbf{0} & \mathbf{A_2} & \mathbf{A_1} & \mathbf{A_0} & \mathbf{0} & \ddots \\ \vdots & \ddots & \ddots & \ddots & \ddots & \ddots \end{bmatrix}, \quad (25)$$

where the matrices $\mathbf{B} = 1 - \alpha$, $\mathbf{E} = (1-\alpha)\mathbf{s}$, and $\mathbf{C} = \alpha\boldsymbol{\beta}$ are the sub-stochastic boundary matrices that track, respectively, the transitions within, to, and from the idle state. The matrices $\mathbf{A_0} = \alpha\mathbf{S}$, $\mathbf{A_1} = \alpha\mathbf{s}\boldsymbol{\beta} + (1-\alpha)\mathbf{S}$, and $\mathbf{A_2} = (1-\alpha)\mathbf{s}\boldsymbol{\beta}$ are of size $N_d \times N_d$ that track, respectively, the upward transitions from q to $q + 1$, the transitions within the same level q, and the downward transitions from $q + 1$ to q.

Remark 2: The queuing system is stable (packets have a finite delay) if the packet departure rate $\frac{S_p}{N_d}$ is higher than the packet arrival rate α.

After ensuring the stability of the queue, the steady-state solution of the queueing model is obtained by solving (26), where $\mathbf{1}$ is a column vector of ones.

$$\boldsymbol{\pi} = \boldsymbol{\pi}\mathbf{P} \quad \text{and} \quad \boldsymbol{\pi}\mathbf{1} = 1. \quad (26)$$

The solution $\boldsymbol{\pi} = [\pi_0 \; \boldsymbol{\pi}_1 \cdots \boldsymbol{\pi}_q \cdots]$ is the joint distribution of the state space (q, d), such that π_0 is the probability of having idle buffer. For $q \geq 1$, the vector $\boldsymbol{\pi}_q$ of length $1 \times N_d$ tracks the probabilities of elapsed time slots, d, since the last attempt transmission of the HoB packet, when there are q packets in the buffer. MAM[7] is used to solve the system in (26) as follows

Theorem 3: The steady-state solution $\boldsymbol{\pi}$ is given by

$$\boldsymbol{\pi}_q = \begin{cases} (1 + \alpha\boldsymbol{\beta}\mathbf{M}(\mathbf{I} - \mathbf{R})^{-1}\mathbf{1})^{-1}, & \text{for } q = 0 \\ \pi_0 \alpha\boldsymbol{\beta}\mathbf{M}, & \text{for } q = 1 \\ \boldsymbol{\pi}_1\mathbf{R}^{q-1}, & \text{for } q \geq 2 \end{cases} \quad (27)$$

where $\mathbf{M} = (\mathbf{I} - \alpha\mathbf{s}\boldsymbol{\beta} - (1-\alpha)\mathbf{S} - \mathbf{R}(1-\alpha)\mathbf{s}\boldsymbol{\beta})^{-1}$, and $\mathbf{R}$ is the rate matrix given by $\mathbf{R} = \alpha\mathbf{S}(\mathbf{I} - \alpha\mathbf{s}\boldsymbol{\beta} - (1-\alpha)\mathbf{S} - \alpha\mathbf{S}\mathbf{1}\boldsymbol{\beta})^{-1}$

Proof: π_0 and $\boldsymbol{\pi}_1$ are found by solving the boundary equation $\boldsymbol{\pi}_1 = \pi_0\mathbf{C} + \boldsymbol{\pi}_1(\mathbf{A_1} + \mathbf{R}\mathbf{A_2})$ and the normalization condition $\pi_0 + \boldsymbol{\pi}_1(\mathbf{I} - \mathbf{R})^{-1}\mathbf{1} = 1$. After that, $\boldsymbol{\pi}_q$ follows from the definition of the rate matrix $\mathbf{R}$ as the minimal non-negative solution of $\mathbf{R} = \mathbf{A_0} + \mathbf{R}\mathbf{A_1} + \mathbf{R}^2\mathbf{A_2}$, and since $\mathbf{A_2}$ is of rank one, an explicit expressions for $\mathbf{R}$ is obtained [66]. ∎

The steady-state solution can be used to investigate certain performance indicators, such as the average queue length as specified by

$$Q_L = \sum_{i=1}^{\infty} i\boldsymbol{\pi}_i\mathbf{1} = \boldsymbol{\pi}_1(\mathbf{I} - \mathbf{R})^{-2}\mathbf{1}. \quad (28)$$

Utilizing Little's Law, the average total delay[8] (queueing and transmission delay) is calculated as

$$Q_W = \frac{\boldsymbol{\pi}_1(\mathbf{I} - \mathbf{R})^{-2}\mathbf{1}}{\alpha}. \quad (29)$$

2) SUC-UL: In the SUC-UL model, the transmission is during the whole time slot duration T_s, and the outage capacity is given by

$$C_{\text{UC}} = \mathbb{P}\left(\text{SINR}_{\text{UC}} > \theta_{\text{UC}}\right) \times \zeta W \log_2\left(1 + \theta_{\text{UC}}\right). \quad (30)$$

Each device attempts to transfer a packet of size L completely during its assigned time slot that yields the SINR threshold in (3). Similarly, a Geo/PH/1 queueing model is studied at each device, where all the equations are identical to the model described in IV-B1. The only variation is the term S_p; here, it refers to the packet transmission success probability derived in Theorem 2 for the SINR threshold specified in (3).

C. Energy Efficiency

To make an objective assessment of both models, the overall energy consumption is considered from both the UAV and devices point of view.

---

[7]The MAM computation is carried out offline to come up with long-term network design parameters (e.g., α and L). These design parameters remain fixed as long as the statistical network parameters (e.g, devices density, UAVs density, and fading distribution) remain constant.

[8]The results of the steady-state solution and average total delay will remain the same if another queuing discipline such as last-come-first-served (LCFS) is utilized [66], [67].

1) URDC-UL : From the UAV viewpoint, the overall energy consumption is separated into propulsion energy and energy related to communication [68]. The power required for communication P_c is considered constant. This power is employed in a variety of tasks, including communication and signal processing circuits, as well as signal transmission and reception. Propulsion energy, on the other hand, is the mechanical energy that is used during hovering or forward movement. Note that communication-related energy is negligible when compared to propulsion energy consumption. According to [68], for a rotary-wing UAV that can hover or move forward with speed v, the propulsion power consumption is given by

$$P_t(v) = P_0\left(1 + \frac{3v^2}{U_{tip}^2}\right) + P_i\left(\sqrt{1 + \frac{v^4}{4v_0^4}} - \frac{v^2}{2v_0^2}\right)^{\frac{1}{2}} + \frac{1}{2}d_0\rho s_r A v^3, \quad (31)$$

where P_0 and P_i are two constants representing the blade profile power and induced power in hovering given by

$$P_0 = \frac{\delta}{8}\rho s_r A\Omega^3 R_r^3 \quad \text{and} \quad P_i = (1 + k_c)\frac{W_u^{\frac{3}{2}}}{\sqrt{2\rho A}}, \quad (32)$$

where W_u is the UAV weight, ρ is the air density, R_r is the rotor radius, A is the rotor disc area, U_{tip} is the tip speed of the rotor blade, v_0 is the mean rotor-induced velocity in hover, d_0 is the fuselage drag ratio, s_r is the rotor solidity, δ is the profile drag coefficient, Ω is the blade angular velocity, and k_c is the incremental correction factor to induced power. By substituting $v = 0$ in (31), we obtain the power consumption during hovering which is a constant given by

$$P_h = P_0 + P_i. \quad (33)$$

For the URDC-UL model, the total energy consumption by the UAV in a single time slot is the traveling energy of the UAV during t_V plus the hovering energy of the UAV during t_{DC} plus communication-related energy during t_{DC} given as

$$E_{\text{DC}_{\text{UAV}}} = P_t\, t_V + P_h\, t_{\text{DC}} + P_c\, t_{\text{DC}}, \quad (34)$$

where P_t is the traveling power at speed v given by (31).

The energy efficiency in bits/Joule is defined as the transmission throughput per unit of energy consumed during a fixed time interval. Accordingly, the energy efficiency in the URDC-UL model from the UAV viewpoint $EE_{\text{DC}_{\text{UAV}}}$ is given by

$$EE_{\text{DC}_{\text{UAV}}} = \frac{C_{\text{DC}} \times T_s}{E_{\text{DC}_{\text{UAV}}}}. \quad (35)$$

Considering only the uplink transmission power, the energy efficiency in the URDC-UL model from the device viewpoint is given by

$$EE_{\text{DC}_{\text{IoT}}} = \frac{C_{\text{DC}} \times T_s}{P \times t_{\text{DC}}}. \quad (36)$$

2) SUC-UL: From the UAV point of view, the total energy consumption in a single time slot is the hovering energy of the UAV during the whole time slot duration T_s, plus communication-related energy during T_s given as

$$E_{\text{UC}_{\text{UAV}}} = P_h\, T_s + P_c\, T_s, \quad (37)$$

and the energy efficiency from the UAV viewpoint in the SUC-UL model $EE_{\text{UC}_{\text{UAV}}}$ is given by

$$EE_{\text{UC}_{\text{UAV}}} = \frac{C_{\text{UC}} \times T_s}{E_{\text{UC}_{\text{UAV}}}} = \frac{C_{\text{UC}}}{P_h + P_c}, \quad (38)$$

TABLE II: Parameters for numerical demonstration.

Parameter Description	Symbol	Value
Hexagonal cell radius	R	651.5 m
UAV height	h	30 m
UAV intensity	λ_u	$0.90689/\text{km}^2$
Device intensity	λ_d	$90.693/\text{km}^2$
Main lobes gain	G_{dM}, G_{uM}	5 dBi
Side lobes gain	G_{dm}, G_{um}	0 dBi
Main lobe beamwidths	θ_d, θ_u	$40°$
Path loss exponents	α_L, α_N	2.5, 4
Gamma RVs shape parameters	m_L, m_N	3, 1
Theoretical-to-practical rate	ζ	0.8
Packet's generation probability	α	0.005
Average number of devices per cell	N	100
Average traveling duration	t_V	6.4365 s
Transmission duration	t_{DC}	6.4365 s
Time slot duration	T_s	12.8729 s
UAV speed	v	22 m/s
UAV acceleration and deceleration	a_u, a_d	11 m/s^2
Bandwidth	W	125 kHz
Noise power	σ^2	-90 dBm
Device transmission power	P	1 mW
UAV communication related power	P_c	50 mW
SD of the horizontal distance	η	20 m
Simulation area	$-$	20000 km^2
UAV weight	W_u	100 N
Air density	ρ	1.225 kg/m^3
Rotor radius	R_r	0.5 m
Rotor disc area	A	0.79 m^2
Tip speed of the rotor blade	U_{tip}	200 m/s
Mean rotor induced velocity in hover	v_0	7.2 m/s
Fuselage drag ratio	d_0	0.3
Rotor solidity	s_r	0.05
Profile drag coefficient	δ	0.012
Blade angular velocity	Ω	400 radians/s
Incremental correction factor	k_c	0.1

while the energy efficiency from the device viewpoint in the SUC-UL model is given by

$$EE_{\text{UC}_{\text{IoT}}} = \frac{C_{\text{UC}} \times T_s}{P \times T_s} = \frac{C_{\text{UC}}}{P}. \tag{39}$$

V. NUMERICAL RESULTS

This section validates the analytical results for success probability by performing Monte Carlo simulations to corroborate the derivations. Then, the two models are compared in terms of outage capacity, delay, and energy efficiency. Furthermore, the effect of other parameters such as the UAV height, t_{DC} duration, and transmission power is discussed. Unless otherwise specified, the results in this section are based on the numerical parameters listed in Table II, where the values of mechanical parameters are taken from [68]. In addition, the environment parameters are given in Table III according to [56]. The t_V value is calculated utilizing proposition 1, and the ratio between t_{DC} and t_V is selected to be unity which provides high gain while ensuring that the total energy consumption during one transmission cycle is still within the practical limits as we will present in this section. Note that the values of t_V, t_{DC}, and T_s remain fixed unless system parameters or devices' locations are changed. Moreover, the number of devices for the queueing analysis N_d is configured to be equal to the mean number of devices in each cell N. As a result, the delay performance is calculated as the average of all cells.

TABLE III: Environment parameters [56]

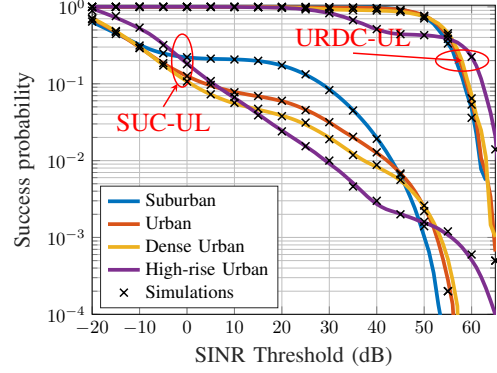| Environment	a	b
Suburban	4.88	0.429
Urban	9.612	0.158
Dense urban	12.081	0.114
High-rise urban	27.23	0.078

Fig. 4: Average success probability for both models.

Fig. 4 illustrates the average probability of success for the URDC-UL and SUC-UL schemes in various environments. The close correspondence between analysis and numerical simulation of the exact network demonstrates the validation of proposed analytical models and particularly, the accuracy of Approximation 1. Moreover, the figure demonstrates that the URDC-UL model has an incredibly high probability of success even at very high SINR thresholds. This result can be exploited to increase the size of the packets L or even to lower the assigned bandwidth W, or more importantly to lower the transmission power of IoT devices while keeping a reliable communication link. Furthermore, the figure demonstrates that the environment affects both the intended and interference links. At very low and very high SINR thresholds, the interference link's influence is prominent, resulting in the maximum success probability for high-rise urban locations. However, for most of the SINR thresholds range, the intended link is the dominant one, resulting in the highest probability of success for the suburban region.
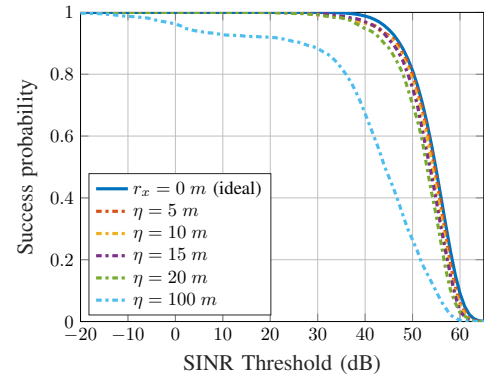
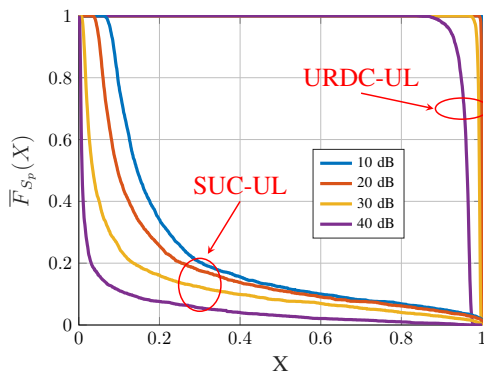Fig. 5: Success probability of URDC-UL model for the suburban area at different η values.

Fig. 6: Meta distribution at $h = 30$ m in a suburban area for different SINR thresholds.
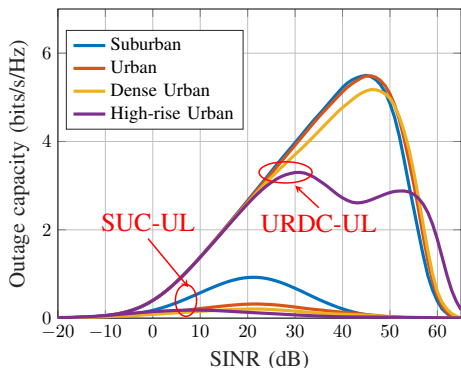

Fig. 7: Average outage capacity for both models.

The success probability in a suburban area is plotted in Fig. 5 for various values of the SD, η, of r_x. By treating r_x as a Gaussian RV, the system covers a more realistic and practical scenario in which P_{LOS} can take values other than 1 depending on the η value. The figure confirms that the URDC-UL model still offers ultra-reliable links at reasonable values for localization error, not only at the ideal LOS probability of 1 (UAV hovering above the device). For the remaining results, we use $\eta = 20$ m, which represents a large localization error. However, the URDC-UL model still preserves the ultra-reliable transmission probability at higher thresholds.

Fig. 6 plots the meta distribution for both models. The results for the URDC-UL scheme show an ultra-reliable and almost unified performance for all devices, while at a high SINR threshold, i.e. 40 dB, there is a slight difference in performance between devices. This result can be explained as follow, the UAVs travel to the devices to offer high quality (i.e., short distance and high LOS probability) intended link for all devices. Moreover, the interference is relieved and randomized due to the unsynchronized movement of the UAVs, which results in low correlated interference at different transmission attempts. Based on the previous two reasons, the URDC-UL scheme guarantees high and unified success probability for all devices. On the other hand, the meta distribution for the SUC-UL model confirms the location-dependent performance among devices, where the devices near the cell center have better performance. The results of the URDC-UL model highlight the device-centric advantage in terms of fairness.

Consequently, all the following results for the URDC-UL scheme can be considered general for any device.

Fig. 7 illustrates the average outage capacity of both the URDC-UL and the SUC-UL models in various environments. The results are consistent with the success probability.

Fig. 8a illustrates the packet delay associated with the URDC-UL model in various environments. The figure demonstrates how the URDC-UL model enables the transmission of large packets (around 11 Mbits) with a finite delay. Additionally, it replicates the success probability results and demonstrates that the high-rise urban environment has the highest delay as higher success probability thresholds are used at these packet sizes in this model. In Fig. 8b, the average packet delay for the SUC-UL model in various environments is illustrated. It replicates the success probability results and demonstrates that the high-rise urban region has the least delay provided that low success probability thresholds are used at these packet sizes.

Results in Fig. 9 illustrate the average outage probability at various elevations in the suburban region. The results clearly show the superiority of the URDC-UL model at different heights. The findings indicate that the outage probability improves with increasing height up to the ideal height with the minimum outage probability. However, as the height increases further, the probability of an outage rapidly increases. This can be explained by the fact that as the height increases, the likelihood of the intended device becoming LOS increases until the optimal height is reached. Any further increase results in a rise in the number of interferer devices with LOS links, which lowers the success probability. It is worth noting that these optimal heights will be lower if the cell size is decreased.

Following validation of the mathematical analysis, the two models will be compared in terms of success probability, outage capacity, packet delay, and energy efficiency. Results are displayed for suburban regions only for brevity; however, other environments will exhibit comparable trends. The performance characteristics are plotted at $h = 30$ and $h = 100$ meters.

Fig. 10 compares the URDC-UL model's outage capacity with the SUC-UL model's average outage capacity. Despite the fact that transmission happens exclusively during the t_{DC} duration in the URDC-UL model and throughout the time slot in the SUC-UL model, the results reveal that the URDC-UL model's outage capacity is always greater than the SUC-UL model's. This demonstrates that the URDC-UL model's higher probability of success is the decisive factor. Additionally, the figure demonstrates that as the height approaches the SUC-UL model's optimal value, the outage capacity improves for the SUC-UL model while it drops for the URDC-UL model. As a result, the advantage of the URDC-UL model over the SUC-UL model decreases around the SUC-UL model's ideal height ($h = 100$ m).

Fig. 11a compares the almost unified success probability of the URDC-UL model with the average success probability of the SUC-UL model at its optimal height ($h = 100$ m), where the shaded region shows the SUC-UL model's SD. The results indicate that the URDC-UL model always has a greater probability of success, whereas the SUC-UL model's performance is location-dependent. Even in the best-case scenario for the SUC-UL model, if a device is positioned
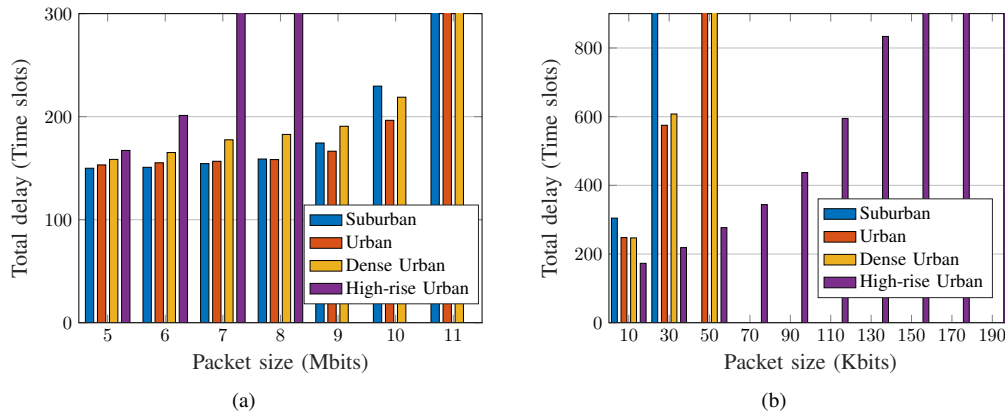
(a)

(b)

Fig. 8: Average packet delay for (a) URDC-UL model and (b) SUC-UL model. Infinite delays are omitted from the figure.
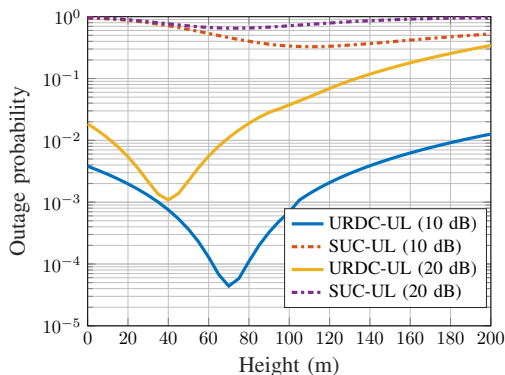

Fig. 9: Effect of height on outage probability in a suburban area.
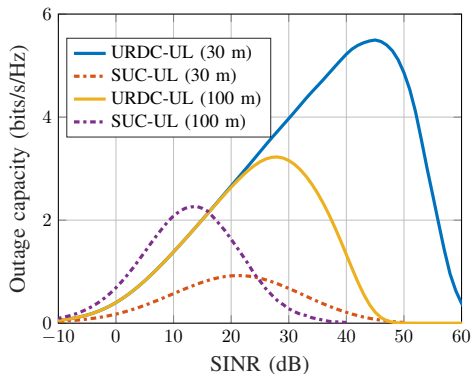

Fig. 10: Outage capacity of the URDC-UL and SUC-UL schemes for a suburban area.

in the cell's center right beneath the UAV, the URDC-UL model has a better success probability. This can be explained by the fact that in the SUC-UL model, all cells always interfere throughout each time slot. However, due to the asynchronous system in the URDC-UL model, some UAVs travel while their selected devices wait and do not contribute to interference. Fig. 11b demonstrates that as the height is reduced to 30 m, the success probability for the SUC-UL model declines while it improves for the URDC-UL model. Moreover, the shaded

region increases, which indicates that around the optimal height ($h = 100$ m) the performance gap between devices is reduced.

Fig. 12 compares the URDC-UL model's delay with the SUC-UL model's average delay. The results indicate that the URDC-UL model has a shorter delay; these findings corroborate the success probability and outage capacity findings. Additionally, the figure demonstrates that large packet sizes are permitted to be transmitted with finite delay in the SUC-UL situation when $h = 100$ m, but significantly smaller packet sizes are permitted when $h = 30$ m. However, in the URDC-UL model, because the delay at $h = 30$ m is less than that at $h = 100$ m, larger packet sizes with a finite delay can be delivered at $h = 30$ m.

Fig. 13 illustrates the propulsion power consumption at various speeds specified in (31). As shown in the figure, there is a speed v at which the Propulsion Power usage is the least. This speed, based on the numerical values used, is $v = 22$ m/s, which was used in this section. According to (31) and (33), the hovering power $P_h = 1.371$ KW, while at $v = 22$ m/s the traveling power $P_t = 0.9363$ KW. From (34) and (37), the total energy consumption by UAV during a single time slot is 17.649 kJ for the SUC-UL model and 15.568 kJ for the URDC-UL model, taking into account additional energy consumed during acceleration before reaching v.

Fig. 14 compares the URDC-UL model's energy efficiency to the SUC-UL model's average energy efficiency versus bandwidth at 20 dB SINR threshold from the UAV viewpoint. Given that the URDC-UL model has a greater outage capacity and consumes less energy on average than the SUC-UL model, it is predicted that the URDC-UL model is more energy efficient. Additionally, the figure demonstrates that as the height approaches the optimal value for the SUC-UL model, the energy efficiency of the SUC-UL model improves. Furthermore, the figure confirms that increasing the bandwidth can greatly enhance energy efficiency. This is predictable as increasing the bandwidth increases the outage capacity while the mechanical energy consumption is unaffected.

Fig. 15 illustrates the ratio of transmission duration t_{DC} to the average traveling time duration t_V versus the average energy efficiency of the URDC-UL and SUC-UL models from
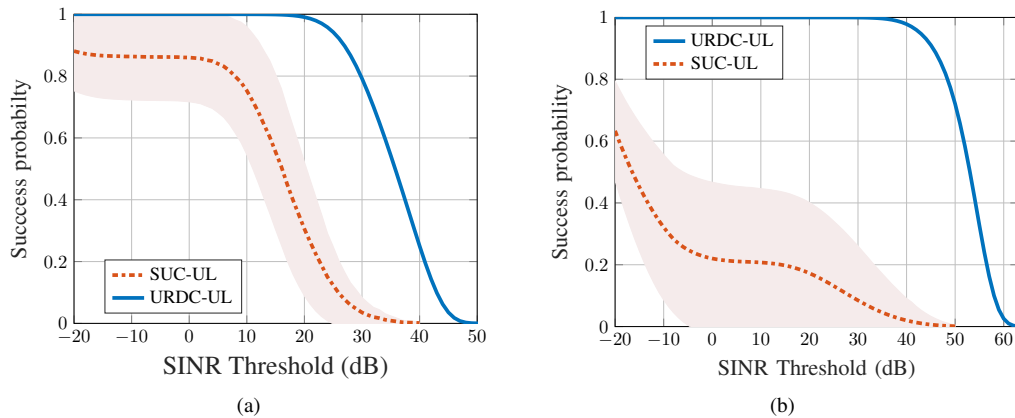
Fig. 11: Success probability for suburban area at (a) $h = 100$ m and (b) $h = 30$ m. The dashed line represents the mean while the shaded area represents the SD of the SUC-UL.
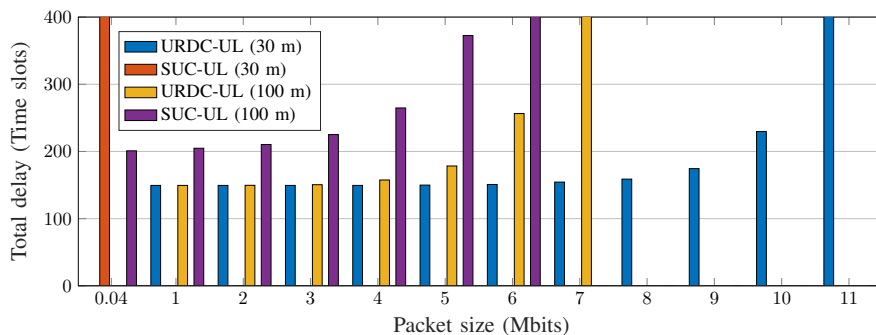

Fig. 12: Packet delay for a suburban area. Infinite delays are omitted from the figure.
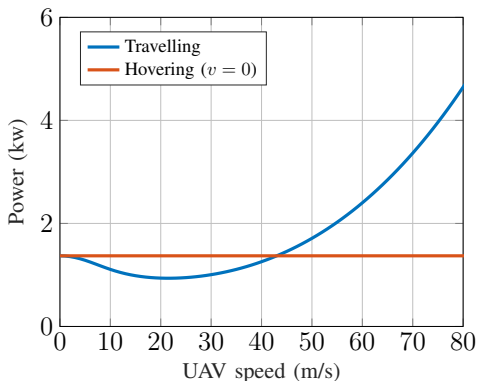

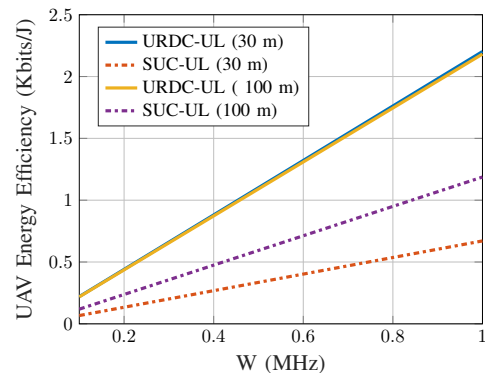Fig. 13: Propulsion Power consumption at different speeds v versus the constant hovering power.

Fig. 14: Energy efficiency from UAV viewpoint versus bandwidth for a suburban area at 20 dB SINR threshold.

the UAV viewpoint at an SINR threshold of 20 dB. The figure demonstrates that as this ratio increases, the URDC-UL model's energy efficiency increases. On the other hand, the SUC-UL model's energy efficiency is always constant for any time slot duration T_s. This implies that increasing the transmission duration t_{DC} increases the gain of the URDC-UL model (i.e., higher rate, higher energy efficiency, and lower delay). However, increasing t_{DC} affects the transmission cycle's overall energy consumption. By increasing t_{DC}, the duration of the total time slot T_s is extended, resulting in an increase

in the total energy consumed during the time slot, E_{DC}. The transmission cycle's total energy usage $E_{cycle} = E_{DC} \times N_d$ must be less than the capacity of the batteries carried by the UAVs. To obtain the numerical findings, in this section, we select a ratio of unity between t_{DC} and t_V. This results in a remarkable gain while maintaining an acceptable energy consumption that can be handled by the available types of batteries.

Fig. 16 plots the outage probability versus transmission power P at SINR threshold = 10 dB for the URDC-UL
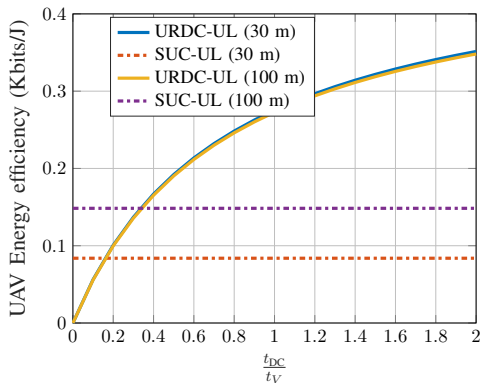
Fig. 15: Transmission to traveling duration ratio vs energy efficiency from UAV viewpoint at 20 dB SINR threshold.
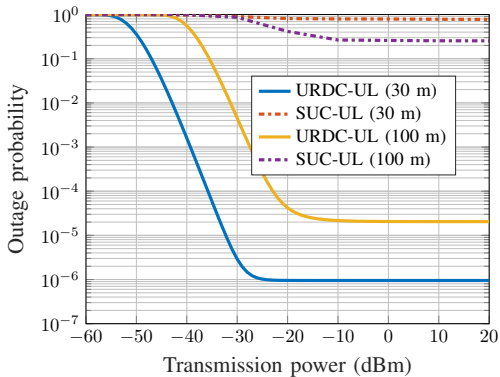

Fig. 16: Outage probability versus transmission power at 10 dB SINR threshold.

Fig. 17: Energy efficiency from IoT device perspective versus transmission power at 10 dB SINR threshold.

model and the average performance of the SUC-UL model. The results demonstrate that the URDC-UL model can reliably provide very low outage probabilities at extremely low transmission power levels. These results illustrate why the URDC-UL model is well-suited for data aggregation in IoT devices, as it overcomes their power limitation issue. Moreover, these results demonstrate that the URDC-UL model offers ultra-reliable service. Note that the outage probability saturates even with increasing transmission power. This can be explained by the transformation of the system from noise-limited to interference-limited, where increasing P only can not enhance the outage probability.

Fig. 17 plots the energy efficiency from the IoT device point of view against the transmission power at 10 dB SINR threshold for the URDC-UL model and the average performance of the SUC-UL model. The results confirm that the URDC-UL model will always offer higher energy efficiency for IoT devices. Moreover, the figure shows that the peak of the energy efficiency for the URDC-UL scheme is at lower transmission powers. This can be explained by the results of Fig. 16 where we can see very low outage probability at extremely low transmission power, owing to the ultra-reliable transmission.

VI. SUMMARY & CONCLUSION

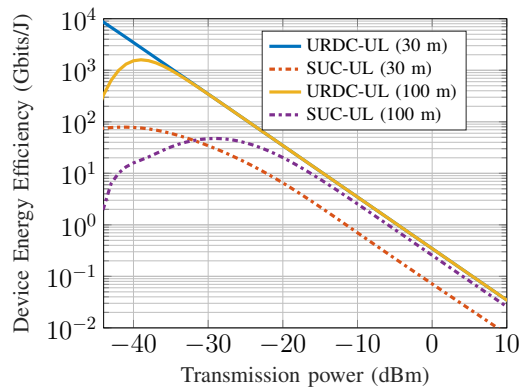This study examines whether it is worthwhile to travel toward IoT devices for data aggregation. A novel spatiotemporal URDC-UL model for data aggregation in large-scale IoT networks employing UAVs, that accounts for interference from other devices, is presented to answer this topic. The UAV in particular navigates to the nearest IoT device and attempts to communicate from the closest distance possible. However, time is lost due to mechanical movement. A second stationary SUC-UL model with comparable parameters is presented for comparison with the proposed model, where the entire duration is allocated for transmission, but the probability of retransmission is increased.

The results indicate that the transmission-to-traveling duration ratio is a crucial design parameter that is constrained by the total amount of energy consumed. In conclusion, by increasing the transmission duration to a suitable value that can be supported by UAV batteries, the proposed URDC-UL model outperforms the SUC-UL model. It delivers a higher probability of success, an improved rate, enhanced energy efficiency, and a shorter delay. In addition, the URDC-UL paradigm assures that performance is almost identical across all devices, regardless of location. However, the SUC-UL model's performance varies by location. Moreover, the proposed URDC-UL model enables IoT devices to greatly reduce their transmission power while maintaining link quality due to the ultra-reliable transmission introduced by the model. This helps preserve the device's battery and addresses a crucial issue in the IoT network design.

APPENDIX A
PROOF OF LEMMA 1

We begin with the LOS interference,

$$\mathcal{L}_{I_L}(s) \stackrel{a}{=} \mathbb{E}_{\boldsymbol{\Phi}_L} \left[\exp\left\{ -s \sum_{x_i \in \boldsymbol{\Phi}_L} PH_{L,i}G_{\epsilon,i}(r_i^2 + h^2)^{\frac{-\alpha_L}{2}} \right\} \right]$$

$$\stackrel{b}{=} \mathbb{E}_r \left[\prod_{x_i \in \boldsymbol{\Phi}_L} \mathbb{E}_{H_L} \exp\left\{ -sPH_{L,i}G_{\epsilon,i}(r_i^2 + h^2)^{\frac{-\alpha_L}{2}} \right\} \right]$$

$$\stackrel{c}{=} \mathbb{E}_r \left[\prod_{x_i \in \boldsymbol{\Phi}_L} \left(1 + \frac{sPG_{\epsilon,i}(r_i^2 + h^2)^{\frac{-\alpha_L}{2}}}{m_L} \right)^{-m_L} \right]$$

$$\stackrel{d}{=} \exp\left\{ -2\pi\lambda_{\mathrm{DC}} \int_{\frac{R}{2}}^{\infty} p_{\mathrm{LOS}}(r) \right.$$
$$\left. \left(1 - \left(1 + \frac{sPG_{\epsilon}(r^2 + h^2)^{\frac{-\alpha_L}{2}}}{m_L} \right)^{-m_L} \right) r dr \right\}.$$
$$(40)$$

(a) follows from the definition of Laplace Transform. (b) follows from the independence between the distributions of channel fading gains and interferers distance. (c) follows from the Gamma distribution's moment-generating function. (d) follows from the definition of probability generating functional (PGFL) in PPP. When a sectored antenna is employed, four discrete probabilities of the antenna gain are available, and the final equation is given by (8). For the NLOS interference, we replace $p_{\mathrm{LOS}}(r)$ by $(1 - p_{\mathrm{LOS}}(r))$, m_L by m_N, and α_L by α_N to get (9).

APPENDIX B
PROOF OF THEOREM 1

The packet's success probability given the intended link is LOS is

$$(S_p|k=L) = \mathbb{P}\left(\frac{PH_{L,o}G_{dM}G_{uM}(r_x^2 + h^2)^{\frac{-\alpha_L}{2}}}{I_L + I_N + \sigma^2} > \theta_{\mathrm{DC}} \right)$$

$$= \mathbb{P}\left(H_{L,o} > \frac{\theta_{\mathrm{DC}}(r_x^2 + h^2)^{\frac{\alpha_L}{2}}(I_L + I_N + \sigma^2)}{PG_{dM}G_{uM}} \right).$$
$$(41)$$

Since $H_{L,o}$ is a Gamma RV, then using Alzer's inequality [69],

$$(S_p|k=L) \approx \sum_{n=1}^{m_L} (-1)^{n+1} \binom{m_L}{n}$$
$$\mathbb{E}\left[\exp\left(-\frac{g_L \, n \, \theta_{\mathrm{DC}} \, (r_x^2 + h^2)^{\frac{\alpha_L}{2}} (I_L + I_N + \sigma^2)}{PG_{dM}G_{uM}} \right) \right],$$
$$(42)$$

where $g_L = m_L(m_L!)^{-\frac{1}{m_L}}$. Since $\boldsymbol{\Phi}_L$ and $\boldsymbol{\Phi}_N$ are independent and utilizing the definition of Laplace Transform, then

$$(S_p|k=L) = \sum_{n=1}^{m_L} (-1)^{n+1} \binom{m_L}{n} \mathcal{L}_{I_L}\left(\frac{g_L \, n \, \theta_{\mathrm{DC}} \, (r_x^2 + h^2)^{\frac{\alpha_L}{2}}}{PG_{dM}G_{uM}} \right)$$
$$\mathcal{L}_{I_N}\left(\frac{g_L \, n \, \theta_{\mathrm{DC}} \, (r_x^2 + h^2)^{\frac{\alpha_L}{2}}}{PG_{dM}G_{uM}} \right) \exp\left(-\frac{g_L \, n \, \theta_{\mathrm{DC}} \, (r_x^2 + h^2)^{\frac{\alpha_L}{2}} \sigma^2}{PG_{dM}G_{uM}} \right).$$
$$(43)$$

Similarly, $(S_p|k=N)$ is formulated by replacing g_L by $g_N = m_N(m_N!)^{-\frac{1}{m_N}}$, m_L by m_N, and α_L by α_N. Finally, by using

the law of total probability and since r_x is a Gaussian RV with zero mean and variance η^2, then

$$S_p = \int_{-\infty}^{\infty} \left[(S_p|k=L)\, p_{\mathrm{LOS}}(r_x) + (S_p|k=N)\, (1 - p_{\mathrm{LOS}}(r_x)) \right]$$
$$\frac{1}{\sqrt{2\pi\eta^2}} \exp\left(\frac{-r_x^2}{2\eta^2} \right) dr_x.$$
$$(44)$$

REFERENCES

[1] X. Cao, P. Yang, M. Alzenad, X. Xi, D. Wu, and H. Yanikomeroglu, "Airborne communication networks: A survey," *IEEE Journal on Selected Areas in Communications*, vol. 36, no. 9, pp. 1907–1926, 2018.

[2] I. Bor-Yaliniz, M. Salem, G. Senerath, and H. Yanikomeroglu, "Is 5G ready for drones: A look into contemporary and prospective wireless networks from a standardization perspective," *IEEE Wireless Communications*, vol. 26, no. 1, pp. 18–27, 2019.

[3] Y. Zeng, Q. Wu, and R. Zhang, "Accessing from the sky: A tutorial on UAV communications for 5G and beyond," *Proceedings of the IEEE*, vol. 107, no. 12, pp. 2327–2375, 2019.

[4] B. Li, Z. Fei, and Y. Zhang, "UAV communications for 5G and beyond: Recent advances and future trends," *IEEE Internet of Things Journal*, vol. 6, no. 2, pp. 2241–2263, 2018.

[5] T. Darwish, G. K. Kurt, H. Yanikomeroglu, M. Bellemare, and G. Lamontagne, "LEO satellites in 5G and beyond networks: A review from a standardization perspective," *arXiv preprint arXiv:2110.08654*, 2021.

[6] G. K. Kurt, M. G. Khoshkholgh, S. Alfattani, A. Ibrahim, T. S. Darwish, M. S. Alam, H. Yanikomeroglu, and A. Yongacoglu, "A vision and framework for the high altitude platform station (HAPS) networks of the future," *IEEE Communications Surveys & Tutorials*, vol. 23, no. 2, pp. 729–779, 2021.

[7] M. S. Alam, G. K. Kurt, H. Yanikomeroglu, P. Zhu, and N. D. Đào, "High altitude platform station based super macro base station constellations," *IEEE Communications Magazine*, vol. 59, no. 1, pp. 103–109, 2021.

[8] M. Mozaffari, W. Saad, M. Bennis, Y.-H. Nam, and M. Debbah, "A tutorial on UAVs for wireless networks: Applications, challenges, and open problems," *IEEE communications surveys & tutorials*, vol. 21, no. 3, pp. 2334–2360, 2019.

[9] X. Lin, V. Yajnanarayana, S. D. Muruganathan, S. Gao, H. Asplund, H.-L. Maattanen, M. Bergstrom, S. Euler, and Y.-P. E. Wang, "The sky is not the limit: LTE for unmanned aerial vehicles," *IEEE Communications Magazine*, vol. 56, no. 4, pp. 204–210, 2018.

[10] A. Azizi, S. Parsaeefard, M. R. Javan, N. Mokari, and H. Yanikomeroglu, "Profit maximization in 5G+ networks with heterogeneous aerial and ground base stations," *IEEE Transactions on Mobile Computing*, vol. 19, no. 10, pp. 2445–2460, 2019.

[11] C. T. Cicek, H. Gultekin, B. Tavli, and H. Yanikomeroglu, "UAV base station location optimization for next generation wireless networks: Overview and future research directions," in *2019 1st International Conference on Unmanned Vehicle Systems-Oman (UVS)*, pp. 1–6, IEEE, 2019.

[12] Y. Zeng and R. Zhang, "Energy-efficient UAV communication with trajectory optimization," *IEEE Transactions on Wireless Communications*, vol. 16, no. 6, pp. 3747–3760, 2017.

[13] M. Ahmad, M. Ali, M. Naeem, A. Ahmed, M. Iqbal, W. Ejaz, and A. Anpalagan, "Device-centric communication in IoT: an energy efficiency perspective," *Transactions on Emerging Telecommunications Technologies*, vol. 31, no. 2, p. e3750, 2020.

[14] F. Jameel, Z. Hamid, F. Jabeen, S. Zeadally, and M. A. Javed, "A survey of device-to-device communications: Research issues and challenges," *IEEE Communications Surveys & Tutorials*, vol. 20, no. 3, pp. 2133–2168, 2018.

[15] A. Masaracchia, Y. Li, K. K. Nguyen, C. Yin, S. R. Khosravirad, D. B. Da Costa, and T. Q. Duong, "UAV-enabled Ultra-Reliable Low-Latency Communications for 6G : A Comprehensive Survey," *IEEE Access*, 2021.

[16] M. Gharbieh, H. ElSawy, A. Bader, and M.-S. Alouini, "Spatiotemporal stochastic modeling of IoT enabled cellular networks: Scalability and stability analysis," *IEEE Transactions on Communications*, vol. 65, no. 8, pp. 3585–3600, 2017.

[17] P. D. Mankar, M. A. Abd-Elmagid, and H. S. Dhillon, "Spatial distribution of the mean peak age of information in wireless networks," *IEEE Transactions on Wireless Communications*, 2021.

[18] Y. Nabil, H. ElSawy, S. Al-Dharrab, H. Mostafa, and H. Attia, "Data aggregation in regular large-scale iot networks: Granularity, reliability, and delay tradeoffs," *IEEE Internet of Things Journal*, vol. 9, no. 18, pp. 17767–17784, 2022.

[19] Y. Zeng, R. Zhang, and T. J. Lim, "Wireless communications with unmanned aerial vehicles: Opportunities and challenges," *IEEE Communications Magazine*, vol. 54, no. 5, pp. 36–42, 2016.

[20] A. Fotouhi, H. Qiang, M. Ding, M. Hassan, L. G. Giordano, A. Garcia-Rodriguez, and J. Yuan, "Survey on UAV cellular communications: Practical aspects, standardization advancements, regulation, and security challenges," *IEEE Communications Surveys & Tutorials*, vol. 21, no. 4, pp. 3417–3442, 2019.

[21] M. Matracia, M. Kishk, and M.-S. Alouini, "Coverage analysis for UAV-assisted cellular networks in rural areas," *IEEE Open Journal of Vehicular Technology*, 2021.

[22] W. Mei, Q. Wu, and R. Zhang, "Cellular-connected UAV: Uplink association, power control and interference coordination," *IEEE Transactions on wireless communications*, vol. 18, no. 11, pp. 5380–5393, 2019.

[23] R. Arshad, L. Lampe, H. ElSawy, and M. J. Hossain, "Integrating UAVs into existing wireless networks: A stochastic geometry approach," in *2018 IEEE Globecom Workshops (GC Wkshps)*, pp. 1–6, IEEE, 2018.

[24] M. Mozaffari, W. Saad, M. Bennis, and M. Debbah, "Mobile unmanned aerial vehicles (UAVs) for energy-efficient Internet of Things communications," *IEEE Transactions on Wireless Communications*, vol. 16, no. 11, pp. 7574–7589, 2017.

[25] M. Mozaffari, W. Saad, M. Bennis, and M. Debbah, "Unmanned aerial vehicle with underlaid device-to-device communications: Performance and tradeoffs," *IEEE Transactions on Wireless Communications*, vol. 15, no. 6, pp. 3949–3963, 2016.

[26] O. M. Bushnaq, A. Celik, H. ElSawy, M.-S. Alouini, and T. Y. Al-Naffouri, "Aeronautical data aggregation and field estimation in IoT networks: Hovering and traveling time dilemma of UAVs," *IEEE Transactions on Wireless Communications*, vol. 18, no. 10, pp. 4620–4635, 2019.

[27] C.-S. Choi, F. Baccelli, and G. de Veciana, "Modeling and analysis of data harvesting architecture based on unmanned aerial vehicles," *IEEE Transactions on Wireless Communications*, vol. 19, no. 3, pp. 1825–1838, 2019.

[28] S. Zhang, J. Liu, and W. Sun, "Stochastic geometric analysis of multiple unmanned aerial vehicle-assisted communications over Internet of Things," *IEEE Internet of Things Journal*, vol. 6, no. 3, pp. 5446–5460, 2019.

[29] Z. Xiong, Y. Zhang, W. Y. B. Lim, J. Kang, D. Niyato, C. Leung, and C. Miao, "UAV-assisted wireless energy and data transfer with deep reinforcement learning," *IEEE Transactions on Cognitive Communications and Networking*, vol. 7, no. 1, pp. 85–99, 2020.

[30] J. S. Ng, W. C. Ng, W. Y. B. Lim, Z. Xiong, D. Niyato, C. Leung, and C. Miao, "UAV-assisted Wireless Power Charging for Efficient Hybrid Coded Edge Computing Network," in *ICC 2022-IEEE International Conference on Communications*, pp. 4037–4042, IEEE, 2022.

[31] Y. Yang, X. Wei, R. Xu, and L. Peng, "Joint Optimization of AoI, SINR, Completeness, and Energy in UAV-Aided SDCNs: Coalition Formation Game and Cooperative Order," *IEEE Transactions on Green Communications and Networking*, vol. 6, no. 1, pp. 265–280, 2021.

[32] Z. Han, Y. Yang, W. Wang, L. Zhou, T. N. Nguyen, and C. Su, "Age Efficient Optimization in UAV-Aided VEC Network: A Game Theory Viewpoint," *IEEE Transactions on Intelligent Transportation Systems*, vol. 23, no. 12, pp. 25287–25296, 2022.

[33] Y. Yang, W. Wang, R. Xu, G. Srivastava, M. Alazab, T. R. Gadekallu, and C. Su, "AoI Optimization for UAV-aided MEC Networks under Channel Access Attacks: A Game Theoretic Viewpoint," in *ICC 2022-IEEE International Conference on Communications*, pp. 1–6, IEEE, 2022.

[34] W. Wang, G. Srivastava, J. C.-W. Lin, Y. Yang, M. Alazab, and T. R. Gadekallu, "Data freshness optimization under CAA in the UAV-aided MECN: a potential game perspective," *IEEE Transactions on Intelligent Transportation Systems*, 2022.

[35] N. Kouzayha, H. Elsawy, H. Dahrouj, K. Alshaikh, T. Y. Al-Naffouri, and M.-S. Alouini, "Analysis of large scale aerial terrestrial networks with mmwave backhauling," *IEEE Transactions on Wireless Communications*, vol. 20, no. 12, pp. 8362–8380, 2021.

[36] G. Hattab and D. Cabric, "Energy-efficient massive IoT shared spectrum access over UAV-enabled cellular networks," *IEEE Transactions on Communications*, vol. 68, no. 9, pp. 5633–5648, 2020.

[37] A. M. Hayajneh, S. A. R. Zaidi, D. C. McLernon, M. Di Renzo, and M. Ghogho, "Performance analysis of UAV enabled disaster recovery networks: A stochastic geometric framework based on cluster processes," *IEEE Access*, vol. 6, pp. 26215–26230, 2018.

[38] Y. Qin, M. A. Kishk, and M.-S. Alouini, "Performance evaluation of UAV-enabled cellular networks with battery-limited drones," *IEEE Communications Letters*, vol. 24, no. 12, pp. 2664–2668, 2020.

[39] M.-A. Lahmeri, M. A. Kishk, and M.-S. Alouini, "Stochastic geometry-based analysis of airborne base stations with laser-powered UAVs," *IEEE Communications Letters*, vol. 24, no. 1, pp. 173–177, 2019.

[40] M. A. Kishk, A. Bader, and M.-S. Alouini, "On the 3-d placement of airborne base stations using tethered UAVs," *IEEE Transactions on Communications*, vol. 68, no. 8, pp. 5202–5215, 2020.

[41] K. Zhu, J. Yang, Y. Zhang, J. Nie, W. Y. B. Lim, H. Zhang, and Z. Xiong, "Aerial Refueling: Scheduling Wireless Energy Charging for UAV Enabled Data Collection," *IEEE Transactions on Green Communications and Networking*, 2022.

[42] P. Popovski, "Ultra-reliable communication in 5G wireless systems," in *1st International Conference on 5G for Ubiquitous Connectivity*, pp. 146–151, IEEE, 2014.

[43] G. J. Sutton, J. Zeng, R. P. Liu, W. Ni, D. N. Nguyen, B. A. Jayawickrama, X. Huang, M. Abolhasan, Z. Zhang, E. Dutkiewicz, *et al.*, "Enabling technologies for ultra-reliable and low latency communications: From PHY and MAC layer perspectives," *IEEE Communications Surveys & Tutorials*, vol. 21, no. 3, pp. 2488–2524, 2019.

[44] K. Wang, C. Pan, H. Ren, W. Xu, L. Zhang, and A. Nallanathan, "Packet error probability and effective throughput for ultra-reliable and low-latency UAV communications," *IEEE Transactions on Communications*, vol. 69, no. 1, pp. 73–84, 2020.

[45] C. She, C. Liu, T. Q. Quek, C. Yang, and Y. Li, "UAV-assisted uplink transmission for ultra-reliable and low-latency communications," in *2018 IEEE International Conference on Communications Workshops (ICC Workshops)*, pp. 1–6, IEEE, 2018.

[46] K. Chen, Y. Wang, Z. Fei, and X. Wang, "Power limited ultra-reliable and low-latency communication in UAV-enabled IoT networks," in *2020 IEEE Wireless Communications and Networking Conference (WCNC)*, pp. 1–6, IEEE, 2020.

[47] Y. Li, C. Yin, T. Do-Duy, A. Masaracchia, and T. Q. Duong, "Aerial Reconfigurable Intelligent Surface-Enabled URLLC UAV Systems," *IEEE Access*, vol. 9, pp. 140248–140257, 2021.

[48] M. M. Azari, F. Rosas, K.-C. Chen, and S. Pollin, "Ultra reliable UAV communication using altitude and cooperation diversity," *IEEE Transactions on Communications*, vol. 66, no. 1, pp. 330–344, 2017.

[49] A. Ranjha and G. Kaddoum, "Quasi-optimization of distance and blocklength in URLLC aided multi-hop UAV relay links," *IEEE Wireless Communications Letters*, vol. 9, no. 3, pp. 306–310, 2019.

[50] A. Han, T. Lv, and X. Zhang, "UAV beamwidth design for ultra-reliable and low-latency communications with NOMA," in *2019 IEEE International Conference on Communications Workshops (ICC Workshops)*, pp. 1–6, IEEE, 2019.

[51] A. Ranjha, G. Kaddoum, and K. Dev, "Facilitating URLLC in UAV-assisted relay systems with multiple-mobile robots for 6G Networks: A prospective of agriculture 4.0," *IEEE Transactions on Industrial Informatics*, vol. 18, no. 7, pp. 4954–4965, 2021.

[52] C. She, C. Liu, T. Q. Quek, C. Yang, and Y. Li, "Ultra-reliable and low-latency communications in unmanned aerial vehicle communication systems," *IEEE Transactions on communications*, vol. 67, no. 5, pp. 3768–3781, 2019.

[53] E. El Haber, H. A. Alameddine, C. Assi, and S. Sharafeddine, "UAV-aided ultra-reliable low-latency computation offloading in future IoT networks," *IEEE Transactions on Communications*, vol. 69, no. 10, pp. 6838–6851, 2021.

[54] X. Xi, X. Cao, P. Yang, J. Chen, T. Q. Quek, and D. Wu, "Network resource allocation for eMBB payload and URLLC control information communication multiplexing in a multi-UAV relay network," *IEEE Transactions on Communications*, vol. 69, no. 3, pp. 1802–1817, 2020.

[55] H. ElSawy, A. Sultan-Salem, M.-S. Alouini, and M. Z. Win, "Modeling and analysis of cellular networks using stochastic geometry: A tutorial," *IEEE Communications Surveys & Tutorials*, vol. 19, no. 1, pp. 167–203, 2016.

[56] A. Al-Hourani, S. Kandeepan, and S. Lardner, "Optimal LAP altitude for maximum coverage," *IEEE Wireless Communications Letters*, vol. 3, no. 6, pp. 569–572, 2014.

[57] J. G. Andrews, T. Bai, M. N. Kulkarni, A. Alkhateeb, A. K. Gupta, and R. W. Heath, "Modeling and analyzing millimeter wave cellular systems," *IEEE Transactions on Communications*, vol. 65, no. 1, pp. 403–430, 2016.

[58] T. Ratnarajah, "On the performance of relay aided millimeter wave networks," *IEEE Journal of Selected Topics in Signal Processing*, 2016.

[59] M. Emara, H. Elsawy, and G. Bauch, "A spatiotemporal model for peak AoI in uplink IoT networks: Time versus event-triggered traffic," *IEEE Internet of Things Journal*, vol. 7, no. 8, pp. 6762–6777, 2020.

[60] M. Gharbieh, H. ElSawy, H.-C. Yang, A. Bader, and M.-S. Alouini, "Spatiotemporal model for uplink IoT traffic: Scheduling and random access paradox," *IEEE Transactions on Wireless Communications*, vol. 17, no. 12, pp. 8357–8372, 2018.

[61] N. Kouzayha, Z. Dawy, J. G. Andrews, and H. ElSawy, "Joint downlink/uplink RF wake-up solution for IoT over cellular networks," *IEEE Transactions on Wireless Communications*, vol. 17, no. 3, pp. 1574–1588, 2017.

[62] M. Haenggi, "The meta distribution of the SIR in Poisson bipolar and cellular networks," *IEEE Transactions on Wireless Communications*, vol. 15, no. 4, pp. 2577–2589, 2015.

[63] J. Gil-Pelaez, "Note on the inversion theorem," *Biometrika*, vol. 38, no. 3-4, pp. 481–482, 1951.

[64] H. Ibrahim, H. Tabassum, and U. T. Nguyen, "The meta distributions of the SIR/SNR and data rate in coexisting sub-6GHz and millimeter-wave cellular networks," *IEEE Open Journal of the Communications Society*, vol. 1, pp. 1213–1229, 2020.

[65] G. George, R. K. Mungara, A. Lozano, and M. Haenggi, "Ergodic spectral efficiency in MIMO cellular networks," *IEEE Transactions on Wireless Communications*, vol. 16, no. 5, pp. 2835–2849, 2017.

[66] A. S. Alfa, *Applied Discrete-Time Queues*. Springer, 2016.

[67] S. K. Bose, *An introduction to queueing systems*. Springer Science & Business Media, 2013.

[68] Y. Zeng, J. Xu, and R. Zhang, "Energy minimization for wireless communication with rotary-wing UAV," *IEEE Transactions on Wireless Communications*, vol. 18, no. 4, pp. 2329–2345, 2019.

[69] H. Alzer, "On some inequalities for the incomplete gamma function," *Mathematics of Computation*, vol. 66, no. 218, pp. 771–778, 1997.